Mechanics Research Communications 114 (2021) 103693

Contents lists available at ScienceDirect

Mechanics Research Communications

journal homepage: www.elsevier.com/locate/mechrescom

On the effect of the ratio between the yield stresses in shear and in uniaxial tension on forming of isotropic materials

Marta C. Oliveira[a,*], Oana Cazacu[b], Nitin Chandola[b], José L. Alves[c], Luís F. Menezes[a]

[a] CEMMPRE, Department of Mechanical Engineering, University of Coimbra, Polo II, Rua Luís Reis Santos, Pinhal de Marrocos, 3030-788 Coimbra, Portugal
[b] Department of Mechanical and Aerospace Engineering, University of Florida, REEF, 1350N. Poquito Rd., Shalimar, FL 32579, USA
[c] MEMS, Department of Mechanical Engineering, University of Minho, Campus de Azurém, 4800-058 Guimarães, Portugal

ARTICLE INFO

Article history:
Received 13 April 2020
Revised 3 March 2021
Accepted 8 April 2021

Keywords:
Plastic isotropy
Isotropic yield function
Finite element method
Sheet forming
Associated flow rule

ABSTRACT

It is generally believed that the choice of the yield criterion used to describe the plastic behaviour of isotropic metallic materials does not affect much the accuracy of the predictions of forming operations. For this reason, the von Mises yield criterion is used for modelling the plastic behaviour. However, according to the von Mises yield criterion, irrespective of the material, the ratio between the yield stresses in simple shear and in uniaxial tension is the same. In this paper, it is presented a numerical study which reveals that even for one of the simplest deep drawing processes, namely the forming of a cylindrical cup, the yielding description influences the predictions of the plastic strains and the final profile of the part. For the description of yielding, an isotropic yield criterion which allows to differentiate between isotropic materials was used. Specifically, this yield criterion involves a parameter α which is expressible solely in terms of the ratio between the yield stresses in shear and in uniaxial tension; for $\alpha = 0$ it reduces to the von Mises yield criterion. The results of the numerical study are revealing and are believed to provide a new point of view when considering material requirements for drawing performance and models to be used for prediction of the plastic behaviour in deep-drawing processes. From the analysis of the loading paths that the materials experience during the forming of the cup, it appears that the prevalent belief that the yielding properties in the tension-tension quadrant of the yield surface dictate the final profile should be reconsidered. Indeed, the simulations results indicate that for isotropic materials characterized by $\alpha > 0$ ($\sigma_T/\tau_Y > \sqrt{3}$), the cup height is greater than for a von Mises material ($\alpha = 0$), which is higher than the one obtained for materials with $\alpha < 0$ ($\sigma_T/\tau_Y < \sqrt{3}$), i.e. lower values of the ratio between the yield stresses in shear and in uniaxial tension lead to greater cup heights. It is shown that this is mainly related to the plastic deformation of the material initially located in the flange region, which is dictated by the shape of the yield surface in the compression-tension quadrant (i.e. normal to the yield surface in the region between uniaxial compression and pure shear stress states).

1. Introduction

Owing to advances in numerical modelling and finite element methods, numerous studies have been devoted to the numerical simulation of forming processes of metallic materials using orthotropic yield functions of increasing levels of complexity (see e.g. [1]). The focus of these works has been put mainly on the improvement of the predictions of the cup height profile, namely the description of the non-uniformity of the height of the cup which is due to the plastic anisotropy of the sheet. However, for any given orthotropic yield criterion, the predicted shape of the yield locus depends strongly on the identification procedure adopted as well as on the type and extent of the data selected for the determination of the anisotropy coefficients. Very recently, it was shown that all orthotropic yield criteria obtained using a linear transformation of the stress tensor can be identified analytically using formulas involving only four yield points or only four Lankford coefficients [2,3]. Moreover, the new equivalent expressions for the Barlat et al. [4] and the Karafillis and Boyce [5] orthotropic yield criteria that were presented in the above referenced papers enable to recognize that these orthotropic yield functions are simple polynomials in terms of the stress components. Nevertheless, the analysis of the stress states that occur during deep drawing using these orthotropic yield functions remains a very complex task. Consequently, it is very difficult to ascertain the importance of capturing certain yielding characteristics and the implications of neglecting others. For metallic sheets for which the plastic anisotropy induced

* Corresponding author.
E-mail address: marta.oliveira@dem.uc.pt (M.C. Oliveira).

https://doi.org/10.1016/j.mechrescom.2021.103693
0093-6413/

by their fabrication process can be neglected, the analysis of forming processes is done with the von Mises yield criterion [6].

The main goal of this study is to improve the understanding of the yielding characteristics that affect the plastic behaviour during deep drawing of isotropic materials. Specifically, the focus is to provide improved understanding of the loading paths that the material experiences and the influence of the yielding description on the predictions of the plastic strains and the plastic strain distribution in the part. To this end, numerical simulations are conducted for a typical forming process: the drawing of a cylindrical cup. We begin with the brief presentation of the isotropic yield criterion used in this study. The details about the cylindrical cup geometry selected and the numerical model are given in Section 3, which also includes the presentation of the results concerning the height and the thickness distribution along the final profile of the part. In Section 4, the evolution of the stress and strain states that the material experiences during the process are analysed in detail. We conclude with a summary of the main findings (Section 5).

2. Cazacu (2018) isotropic yield criterion

From experimental observations that the extrusion force depends only on the shear stresses, and earlier studies of Coulomb on failure of soils, Tresca arrived at the conclusion that a material deforms plastically once the maximum shear stress reaches a critical threshold [7]. In 1913, von Mises [6] proposed an isotropic yield criterion valid for general three-dimensional loadings, which is quadratic in stresses and insensitive to hydrostatic pressure. This criterion has the simplest mathematical form compatible to the invariance requirements dictated by isotropy (for overviews of the early contributions to the mathematical theory of plasticity see also the monographs of Prager and Hodge [8], and Cristescu [9]). An isotropic yield criterion that involves both the invariants of the stress deviator was proposed by Drucker [10]. It was shown that this criterion captures the mechanical response of certain aluminium alloys with greater accuracy than the ones proposed by Tresca and von Mises (see [11]). For more details and analysis of the capabilities of Drucker's criterion for combined tension-torsion loadings, see for example the monograph of Cazacu et al. [12].

In this paper, we consider the isotropic form of Cazacu's [11] yield criterion, which is expressed as:

$$J_2^4 - \alpha J_2 J_3^2 = \tau_Y^8, \tag{1}$$

where J_2 and J_3 denote the second and third-invariants of the deviator of the Cauchy stress tensor $\boldsymbol{\sigma}$, defined as $\mathbf{s} = \boldsymbol{\sigma} - (\mathrm{tr}\boldsymbol{\sigma}/3)\mathbf{I}$, where tr denotes the trace operator and $\mathbf{I}$ the second-order identity tensor. In Eq. (1), τ_Y denotes the yield stress in pure shear, and α is a material constant. This constant is expressible only in terms of the ratio between τ_Y and σ_T, the yield stress in uniaxial tension, as:

$$\alpha = \frac{27}{4}\left[1 - \left(\frac{\sqrt{3}\tau_Y}{\sigma_T}\right)^8\right]. \tag{2}$$

It can be easily shown that if the parameter α belongs to the following range:

$$\frac{-27}{5} \le \alpha \le 3, \tag{3}$$

the yield function is convex (see [11]). Note that for $\alpha = 0$, the von Mises yield criterion is recovered. For $\alpha > 0$, the yield criterion predicts $\sigma_T > \sqrt{3}\tau_Y$ and the corresponding yield surface is interior to the von Mises one; on the other hand, for $\alpha < 0$, the yield criterion predicts $\sigma_T < \sqrt{3}\tau_Y$ and the corresponding yield surface is exterior to the von Mises one.

Fig. 1 shows the projection of the yield surface given by Eq. (1) in the biaxial plane (i.e. a plane corresponding to one of the eigenvalues of the stress tensor being equal to zero) for several values of the parameter α. In this figure, the principal stresses are denoted by σ_{RD} and σ_{TD}. This is done in order to facilitate the discussion and analysis of the forming results presented in the next section. For isotropic sheets, the rolling direction (RD) is no longer a preferential direction of deformation (just a reference direction in the plane of the sheet) while the transverse direction (TD) is the direction normal to RD in the plane of the sheet.

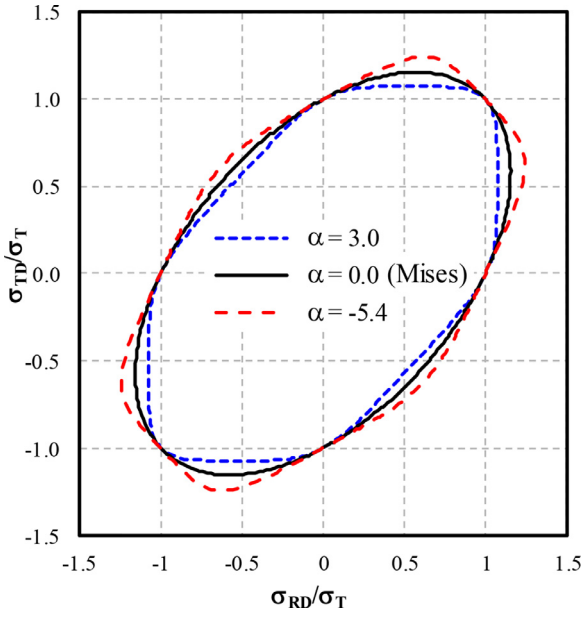

Fig. 1. Biaxial yield surface according to the proposed isotropic yield criterion given by Eq. (1) for different values of the parameter α.

Note that for $\alpha = 3.0$, the curvature of the yield surface is zero for shear loadings, while for $\alpha = -5.4$ this occurs for axisymmetric stress states. In summary, Fig. 1 highlights the fact that this criterion differentiates between materials characterized by different ratios between τ_Y and σ_T, whereas according to the von Mises criterion ($\alpha = 0$) this ratio is fixed.

As previously mentioned, although the drawing of a cylindrical cup is a rather simple forming process, it puts into evidence phenomena that are encountered in more complex deep drawing processes. For this reason, in this paper we focus on the modelling of the cup forming process. Specifically, the influence of the shape of the yield locus on the geometry of the fully drawn cup is investigated. For this purpose, numerical simulations using an elastoplastic model with yielding described by the criterion given by Eq. (1), considering an associated flow rule, and isotropic hardening were conducted.

3. Numerical simulation of the cylindrical cup drawing

The tools selected for the cylindrical cup example have the following dimensions: die and the punch diameters of 62.4 and 60 mm, respectively; shoulder radius of 10 mm for the die and 5 mm for the punch. The blank is circular with a diameter of 120 mm and a nominal thickness of 1.0 mm. In order to minimize the occurrence of stress components normal to the sheet plane in the flange region, the simulations were performed considering a constant value for the gap between the blank-holder and the die (see Fig. 2). In order to avoid the occurrence of any ironing of the cup's wall, the punch height was assumed equal to 17 mm, i.e. the gap of 1.2 mm between the punch and the die is only valid until this height. The contact was assumed frictionless.

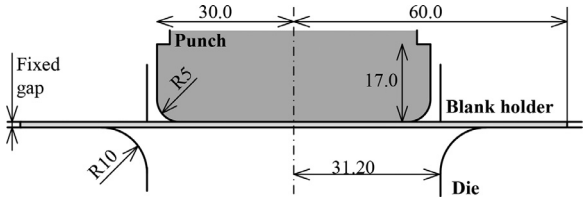

Fig. 2. Schematic representation of the forming tools used in the cup drawing simulations (dimensions in mm).

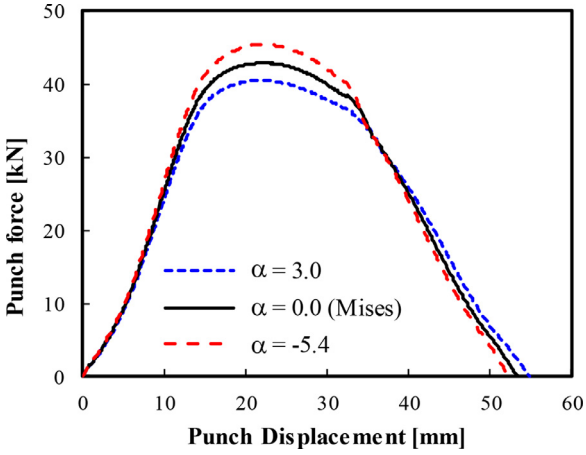

Fig. 3. Evolution of the punch force with displacement for materials characterized by $\alpha = -5.4$ and $\alpha = 3.0$ in comparison with a von Mises material ($\alpha = 0$).

The finite element (FE) simulations were conducted for materials characterized by $\alpha = 3.0$, $\alpha = -5.4$, and $\alpha = 0.0$ (von Mises). Isotropic elastic behaviour was considered, with Young modulus, E, of 210 GPa and Poisson ratio, ν, of 0.3. As previously mentioned, the hardening behaviour is considered to be isotropic and governed by the equivalent plastic strain, $\bar{\varepsilon}^{p}$. Therefore,

$$\bar{\sigma} = Y(\bar{\varepsilon}^{p}), \tag{4}$$

where $\bar{\sigma}$ is the equivalent stress associated with the yield criterion given by Eq. (1) and $\bar{\varepsilon}^{p}$ is the work-equivalent measure of $\bar{\sigma}$. A power-law variation was assumed for the yield stress, Y, i.e.:

$$Y = A(\varepsilon_0 + \bar{\varepsilon}^{p})^{n} \tag{5}$$

where A= 529.6 MPa, ε_0= 0.0044 and n = 0.268 (initial yield stress equal to 123.7 MPa). Moreover, an associated flow rule was adopted.

The blank was discretized with 8-node hexahedra solid finite elements, combined with a selective reduced integration technique [13]. Due to geometrical and material symmetries, only one-fourth of the blank was considered in the model, with a total of 15,982 elements (24,402 nodes). Two layers (4 Gauss points) of elements through the thickness were used, to allow an accurate evaluation of the contact forces and the stress gradients through the thickness. All numerical simulations were performed with DD3IMP in-house finite element solver [14,15].

Fig. 3 presents the punch force vs. displacement. Note that the highest value for the maximum force is attained for the material with $\alpha = -5.4$ and the minimum for the material with $\alpha = 3.0$. The blanks lost contact with the blank-holder for a punch displacement of around 35 mm. The slight difference in the punch displacement value for which the loss of contact occurred is consistent with the difference in the cup height between the three materials (see Fig. 4). The difference in the final cup height between materials is also reflected in the differences between the final punch displacement (i.e. the displacement at which the punch force becomes null). Fig. 4 presents the evolution of the cup height

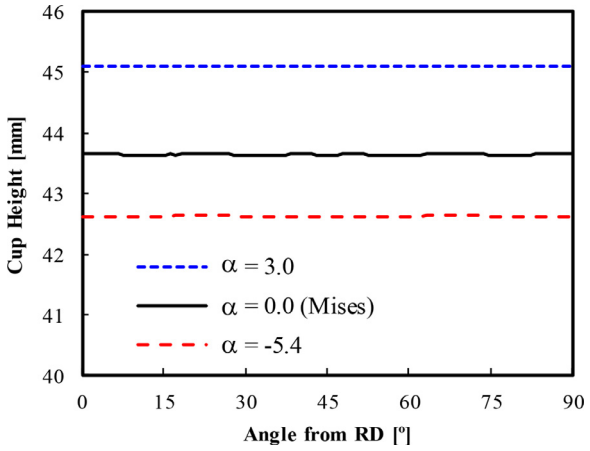

Fig. 4. Evolution of the cup height with the angle from the RD for materials characterized by $\alpha = -5.4$ and $\alpha = 3.0$ in comparison with a von Mises material ($\alpha = 0$).

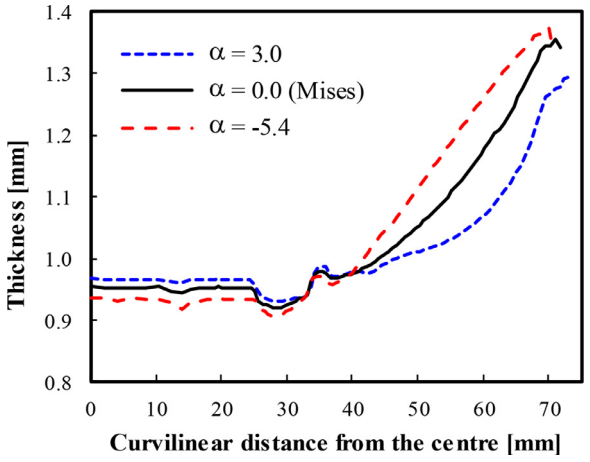

Fig. 5. Thickness evolution from the centre to the wall in fully drawn cups of materials characterized by $\alpha = -5.4$ and $\alpha = 3.0$ in comparison with a von Mises material (α=0.0).

as a function of the angle from the RD. As expected, the yield criterion being isotropic there is no variation in the cup height along its circumference (see Fig. 4). However, it is to be noted that the height of the fully drawn cup depends on the parameter α. The greatest height is obtained for the material with $\alpha = 3.0$, while the smallest height corresponds to the material with $\alpha = -5.4$.

Fig. 5 presents the thickness distribution along the wall of the fully drawn cups (i.e. at the end of the forming process). Note that the predicted distribution presents the usual trend (see e.g. [16]), i.e. constant thickness at the bottom of the cup and minimum in the zone corresponding to the transition between the punch radii and the vertical wall. Note also that the thickness increase along the vertical wall of each cup. It is worth noting that of the three materials, the material with $\alpha = -5.4$ presents most thinning in the bottom region of the cup and the largest increase in the thickness at the wall. However, this material did not accommodate well plastic strains during the process, i.e. the thinning at the bottom was not sufficient to compensate by plastic incompressibility the overall increase in the thickness of the cup's wall resulting in this material having the lowest cup (see Fig. 4). The absolute difference between the thickness at the same location in the cup with respect to the von Mises material is similar for the materials with $\alpha = 3.0$ and $\alpha = -5.4$, respectively. Specifically, for the material with $\alpha = 3$, the cup bottom is slightly thicker than for a von Mises material (~ 2%) while it experienced less increase in thickness at

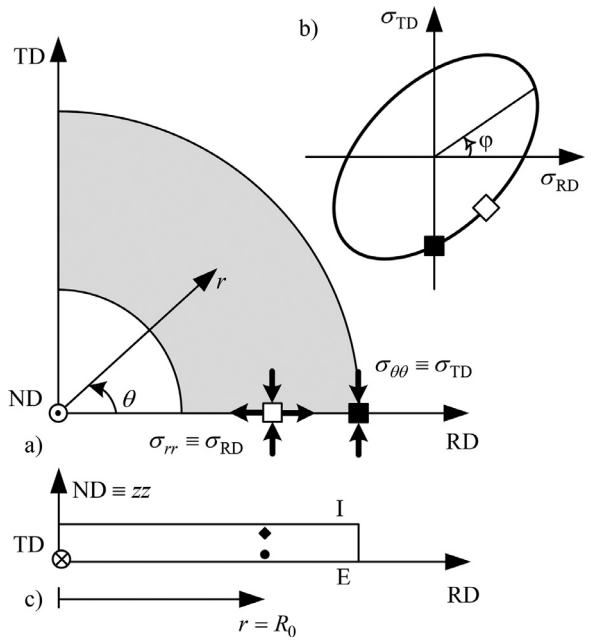

Fig. 6. Analysis of the stress states for material points located in the flange: (a) definition of the coordinate systems; (b) schematic representation of the stress states on the cross-section of the yield surface (adapted from Yoon et al. [17]); and (c) position of the material points considered for the analysis of the strain and stress paths (note that the blank thickness is exaggerated).

the wall (about 10%). In contrast, for the material with $\alpha = -5.4$, at the bottom the cup thickness is lower than that of a von Mises material (~2%) while at the vertical wall it is higher (almost 8%).

As an example, in the Appendix are presented simulation results for the same materials obtained using a Voce-type hardening law. Note that the same conclusions can be reached concerning the influence of the ratio between the yield stresses in pure shear and uniaxial tension (i.e. the value of α). This indicates that the isotropic hardening law has a marginal influence on the cup height and the thickness distribution. It is thus confirmed that the final cup profile and thickness are mainly controlled by the shape of the yield locus.

4. Analysis of the F.E. results and discussion

In order to gain understanding of the reasons for the differences in the height and in the thickness of the cups, we analyse what happens in the flange during this forming process. Fig. 6(a) shows a schematic representation of the stress states occurring in the flange, using two coordinate systems: one is associated with the Cartesian orthogonal system (RD; TD; ND) where ND denotes the through-thickness direction (or normal to the plane of the sheet), while the other is a cylindrical coordinate system, which is most appropriate for analysing the geometry of the cup. Note that since the materials are isotropic, it is sufficient to analyse the mechanical response for materials points located along the RD direction.

As shown in Fig. 6, the points located on the exterior side of the flange (initial radius$R_0 = 60$ mm) are subjected to compression in the TD $\equiv \theta$ direction, while the interior points (i.e. with smaller R_0 values) will be subjected to tension in the radial direction, and compression in the circumferential direction; the ratio between the circumferential ($\sigma_{\theta\theta} \equiv \sigma_{TD}$) and the radial ($\sigma_{rr} \equiv \sigma_{RD}$) stress components depending on the location along the RD. Moreover, this ratio evolves during the forming process. Nevertheless, as long as the stress component normal to the sheet plane (i.e. $\sigma_{zz} \equiv \sigma_{ND}$), is kept close to zero, the shear stresses can be neglected, so the stress state will be located in the fourth quadrant of the yield surface (tension-compression quadrant) in the $\sigma_{RD} - \sigma_{TD}$ plane, as illustrated in Fig. 6(b).

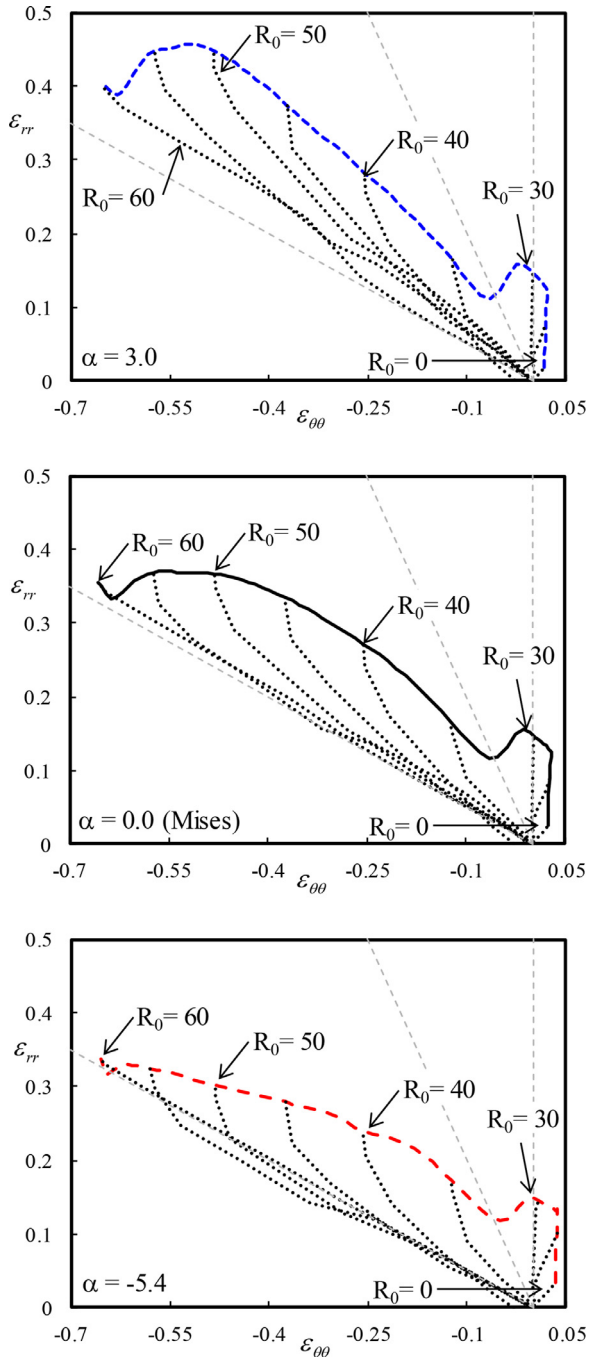

Fig. 7. Comparison of the major-minor strains at the end of the forming process and strain-path followed for nine material points (small dashed lines) located on the exterior (E) side of the cup for materials characterized by different values of the parameter α: (a) $\alpha = 3.0$; (b) $\alpha = 0.0$ (von Mises material) and (c) $\alpha = -5.4$, respectively.

The process conditions adopted are such that the punch is initially located at $z = 1$ mm, and it moves downward (negative z values, see Fig. 6(c)). Our analysis of the stress and strain paths will be performed for integration points (Gauss points) located close to the top and bottom surfaces of the flange. Since in the forming process the material points initially located on the top surface of the flange will end up in the interior part of the cup, these material points are designated with the label "I"; the material points

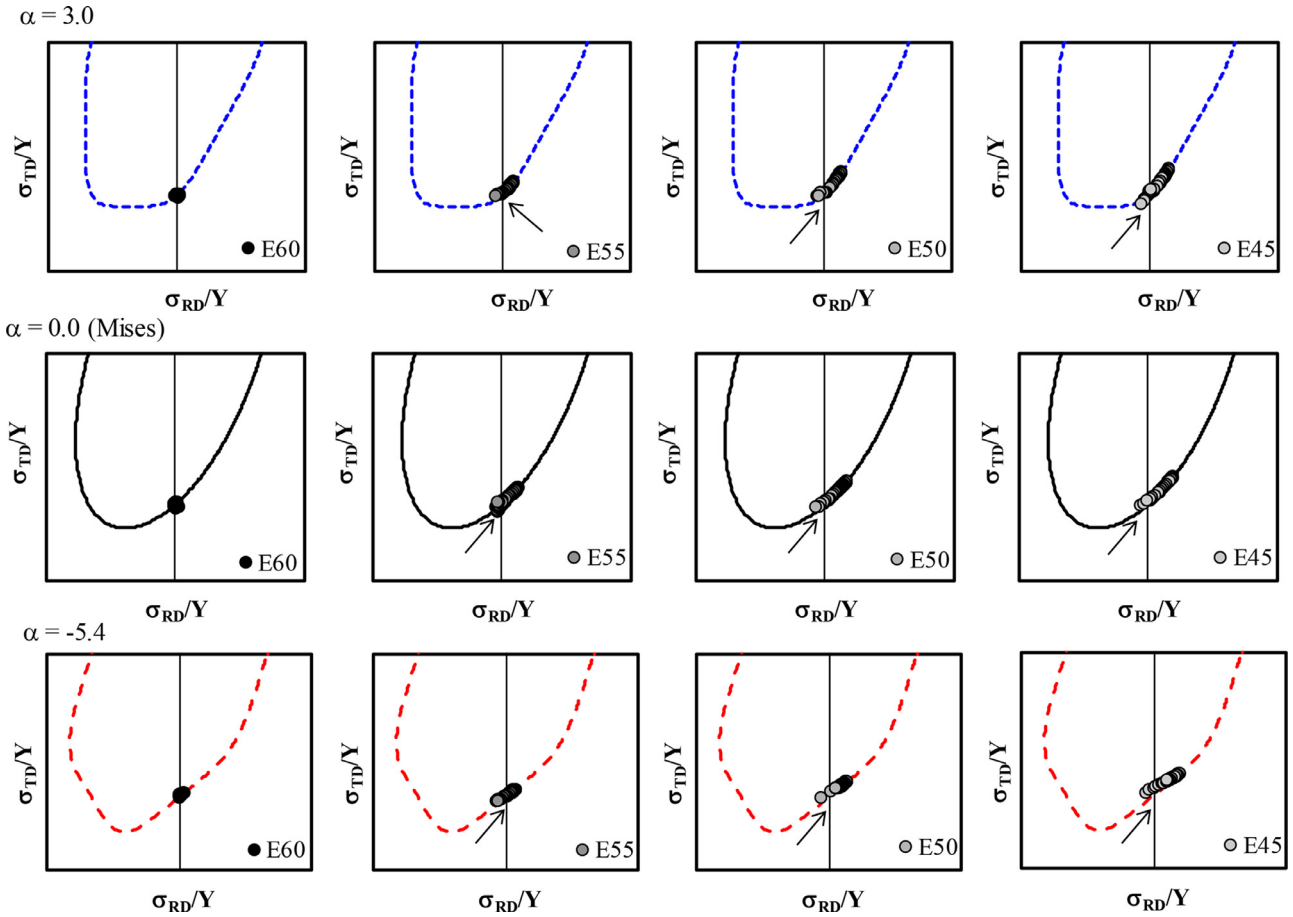

Fig. 8. Predicted evolution of the stress state for four material points, located on the exterior part of the cup (E) for materials characterized by different values of the parameter α. The arrows mark the stress states corresponding to the onset of plastic deformation.

which are initially located on the bottom surface of the flange will end up on the exterior part, and will be referred to with label "E". The bending along the die radius results in $\sigma_{rr} \equiv \sigma_{RD}$ being tensile for the I material points, and compressive for the E points. Finally, we analyse the stress states experienced during the process for points that are initially located between $R_0 = 60$ mm (outer surface) and $R_0 = 25$ mm, with increments of 5 mm (see Fig. 6(c)). Note that, since the punch diameter is of 60 mm, the point initially at $R_0 = 25$ mm will be located at the bottom of the cup.

In order to gain an overall idea of the plastic strains distribution, in Fig. 7 are the major and minor in-plane strains at the end of the forming process, for the material points located in the exterior part of the cup. Note that the major (positive) and the minor (negative) strains are associated with the radial, ε_{rr}, and the circumferential, $\varepsilon_{\theta\theta}$, directions, respectively. The minimum negative value for the $\varepsilon_{\theta\theta}$ strain is similar for the three materials, because it is related to the change in the blank radius. Nevertheless, the maximum value of the ε_{rr} strain is quite different, particularly along the cup wall, i.e. (initial location in the blank between $R_0 = 60$ mm and $R_0 = 40$ mm).

As mentioned, the evolution of the major and minor strain during the process is analysed for material points located on the exterior surface, having different initial radial coordinate (see Fig. 6(c)). The results are shown in Fig. 7 for material points initially located in the blank between $R_0 = 60$ mm and $R_0 = 25$ mm (increments of 5 mm). Moreover, the strain path for the material point located at the centre is also shown, for all three cups. The simulation results show that this material point (R_0= 0 mm) follows an equibiaxial strain path. However, the other points located at the bottom region are subject to strain paths in between the equibiaxial strain and the plane strain (see points with R_0= 25 mm and R_0= 30 mm). Most importantly, the points initially located in the flange, follow a strain path close to uniaxial compression along θ (see the grey dashed line used for reference), the deviation from the uniaxial compression path depending on α. Nevertheless, it is possible to state that for the material with $\alpha = 3.0$ the ratios between the minor ($\varepsilon_{\theta\theta}$) and the major ($\varepsilon_{rr}$) strains have absolute values higher than for the von Mises material ($\alpha = 0$) and the material with $\alpha = -5.4$. This means that for the same decrease in the initial blank radius, the material with $\alpha = 3.0$ experiences a higher deformation in the radial direction and, consequently, a lower deformation in the thickness direction (i.e. less thickening). This is consistent with the FE results presented in Fig. 5.

In order to better understand the differences in the strain distributions in the three materials during the process, the stress evolution during the forming process was also analysed for the same material points (i.e. at Gauss points located closer to the exterior and interior surfaces, as shown in Fig. 6(c)). Specifically, we monitored the stress components for material points initially located at $R_0 = 60$ mm, 55 mm, 50 mm and 45 mm, i.e. close to the exterior (E) and the interior surface (I), respectively. All the stress components other than σ_{rr} and $\sigma_{\theta\theta}$ have negligible values. These stress components normalized by the corresponding value of flow stress, Y, are shown for each material point on the respective yield surfaces in the $\sigma_{RD} - \sigma_{TD}$ plane. Fig. 8 and 9 present the results for the material points located close to the exterior (E) and interior surface, respectively. Note that for material points located on the exterior surface of the cup, the circumferential compression com-

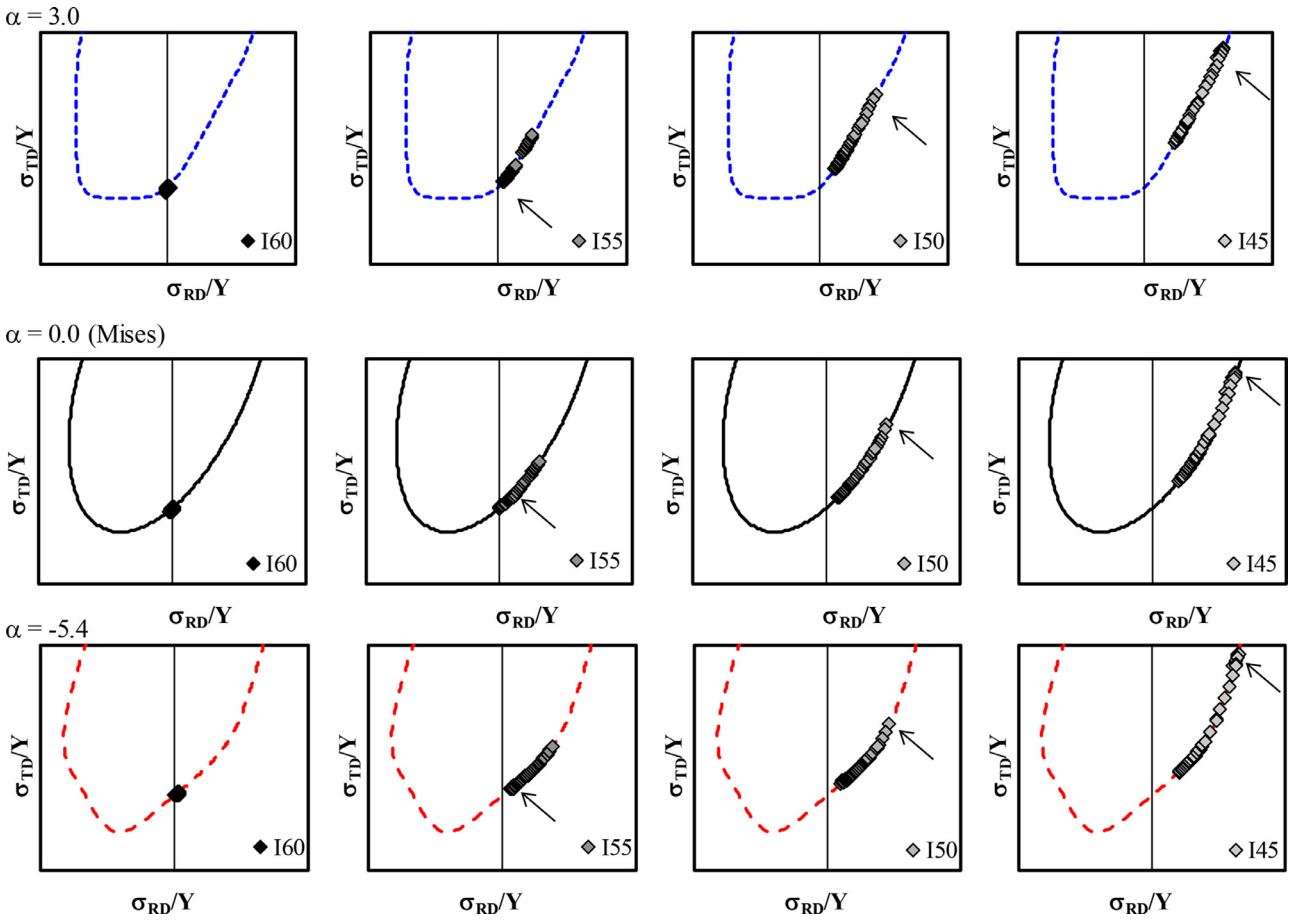

Fig. 9. Evolution of the stress state predicted for four material points, located in the interior part of the cup (I) for materials characterized by different values of the parameter α. The arrows mark the stress states corresponding to the onset of plastic deformation.

ponent $\sigma_{\theta\theta} \equiv \sigma_{\mathrm{TD}}$ has always an absolute value higher than the radial $\sigma_{rr} \equiv \sigma_{\mathrm{RD}}$. However, for material points located on the interior surface, the $\sigma_{rr} \equiv \sigma_{\mathrm{RD}}$ component can have a value higher than the absolute value of the $\sigma_{\theta\theta} \equiv \sigma_{\mathrm{TD}}$ component, particularly when the material starts to deform plastically. Overall, the range of stress states experienced by each material point is similar, irrespective of the material (i.e. the value adopted for α).

For the same material points for which the stress paths were plotted in Figs. 8 and 9, the ratio between the circumferential and the radial strains, $\varepsilon_{\theta\theta}/\varepsilon_{rr}$ are depicted in Fig. 10. Since the points located at R_0= 60 mm are subjected to compression in the circumferential direction, it means that for these points this ratio should be equal to −2. Fig. 10 shows that irrespective of the material, this value of the $\varepsilon_{\theta\theta}/\varepsilon_{rr}$ ratio is indeed attained as soon as plastic deformation occurs, and $\varepsilon_{\theta\theta}/\varepsilon_{rr}$remains practically constant during the process. For the other material points, for similar values for the circumferential strain $\varepsilon_{\theta\theta}$, the radial strain ε_{rr} increases. This increase in the absolute value of $\varepsilon_{\theta\theta}/\varepsilon_{rr}$ is more pronounced for the material characterized by $\alpha = 3.0$. On the other hand, for the material characterized by $\alpha = -5.4$ the $\varepsilon_{\theta\theta}/\varepsilon_{rr}$ ratio is close to −2.0, whatever the ratio between the radial and the circumferential stress components. These results are consistent with the ones presented in Fig. 7(a).

The ratio between the radial and the thickness strain, $\varepsilon_{rr}/\varepsilon_{zz}$, is shown in Fig. 11, for material points located on the exterior and interior surface. Since the points located at R_0= 60 mm are subjected to compression in the circumferential direction, the $\varepsilon_{rr}/\varepsilon_{zz}$ ratio should be equal to 1.0. Irrespective of the material, the results in Fig. 11 show that $\varepsilon_{rr}/\varepsilon_{zz}$=1.0 as soon as plastic deformation occurs, and this ratio remains constant. For the other material points closer to the centre (i.e. away from the flange end), with the increase of the radial stress component, the ratio $\varepsilon_{rr}/\varepsilon_{zz}$ becomes greater than 1.0, which means that either the radial strain increases and/or the thickness strain decreases. Note that the increase of the $\varepsilon_{rr}/\varepsilon_{zz}$ ratio is particularly pronounced for the material characterized by $\alpha = 3.0$, while it remains almost equal to 1.0 for the material with $\alpha = -5.4$.

Based on the analysis of the $\varepsilon_{\theta\theta}/\varepsilon_{rr}$ ratio (see Fig. 10) it may be concluded that the material with $\alpha = 3.0$ experiences a higher increase in the radial strain than the other materials. However, the pronounced increase of the ratio $\varepsilon_{rr}/\varepsilon_{zz}$ is correlated to the fact that for this material there is less thickening of the flange (see Fig. 5). Indeed, for the material with $\alpha = 3.0$, the points flowing from the flange into the die cavity have a reduced increase of thickness, whereas the reverse holds true for the material characterized by $\alpha = -5.4$. Since the radial strain is slightly higher for the material with $\alpha = 3.0$, its cup height is the highest (see Fig. 4).

It is also worth examining whether the FE results presented above are consistent with the plastic strain ratios that can be obtained analytically for biaxial loadings (i.e. in the $\sigma_{\mathrm{RD}} - \sigma_{\mathrm{TD}}$ plane) using Eq. (1) and the normality rule. Fig. 12 shows the evolution of the strain ratios as a function of the applied loading, where $\tan\phi = \sigma_{\mathrm{RD}}/\sigma_{\mathrm{TD}}$ (see Fig. 6(b)). The strain ratios represented in this figure were obtained by direct analytical calculations for loadings in the fourth and first quadrant of the yield surface, i.e. $\phi \in [-90°, 90°]$.

The strain ratio, $\varepsilon_{\mathrm{TD}}/\varepsilon_{\mathrm{RD}}$, is null for plane strain states such that $\varepsilon_{\mathrm{TD}} = 0$, it is equal to −1.0 for pure shear, and it has an infinite

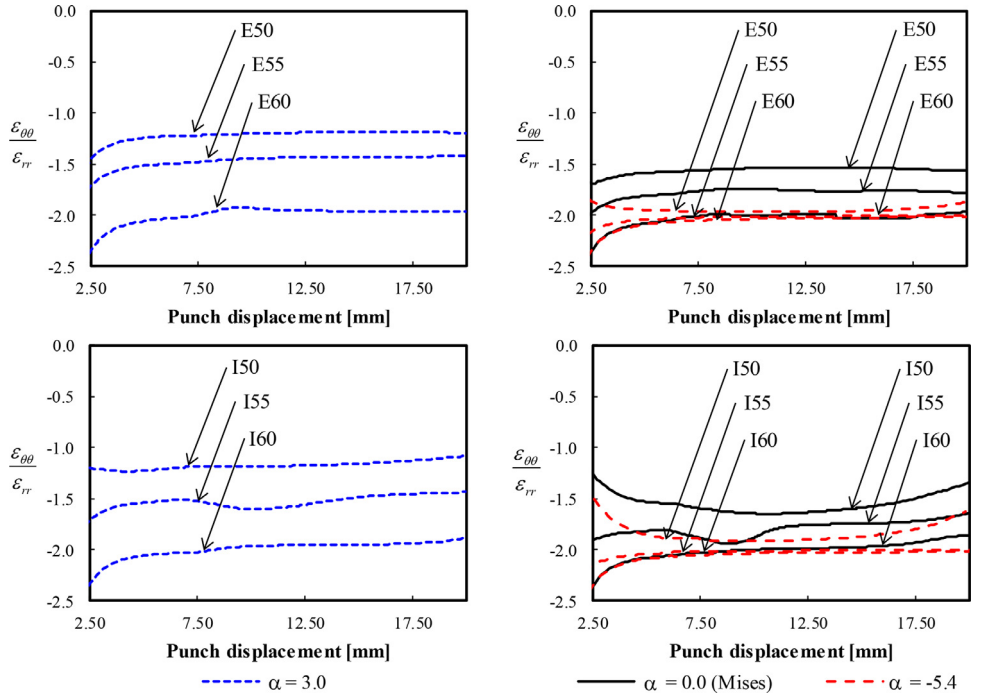

Fig. 10. Evolution of the ratio between the predicted circumferential and radial strains with the punch displacement for three material points located on the exterior part of the cup (E) and three material points located on the interior part of the cup (I) for materials characterized by different values of the parameter α: $\alpha = 3.0$ (left), $\alpha = 0.0$ (von Mises) and $\alpha = -5.4$ (right).

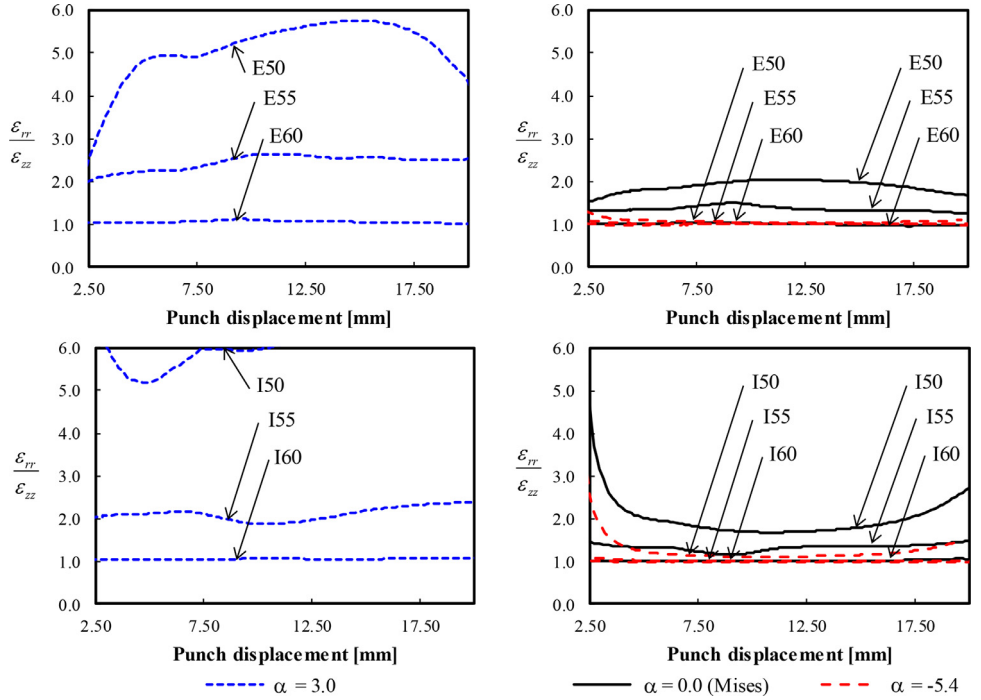

Fig. 11. Evolution of the ratio between the predicted radial and thickness strains with the punch displacement, for three material points located on the exterior part of the cup (E) and three material points located on the interior part of the cup (I) for materials characterized by different values of the parameter α: $\alpha = 3.0$ (left), $\alpha = 0.0$ (von Mises) and $\alpha = -5.4$ (right).

value for plane strain such that $\varepsilon_{RD} = 0$ (see Fig. 12(a)). It is worth noting the different trend in the $\varepsilon_{TD}/\varepsilon_{RD}$ ratio for the three materials considered (see Fig. 12(a)). Given that for isotropic materials, the principal directions for stresses and strains coincide, it can be considered that for the material points analysed on the three cups: $\varepsilon_{\theta\theta} \equiv \varepsilon_{TD}$ and $\varepsilon_{rr} \equiv \varepsilon_{RD}$. Note that the FE results presented in Fig. 10 corroborate with the evolution presented in Fig. 12(a). All six material points are mainly subjected to loadings between uniaxial compression along TD ($\phi = -90°$) and pure shear ($\phi = -45°$). With the increase of the radial stress component, for the material with $\alpha = 3.0$, the $\varepsilon_{TD}/\varepsilon_{RD}$ strain ratio tends rapidly to -1.0. On the other hand, for the material with $\alpha = -5.4$, this strain ratio is closer to -2.0, for a wider range of loading directions (stress ratios).

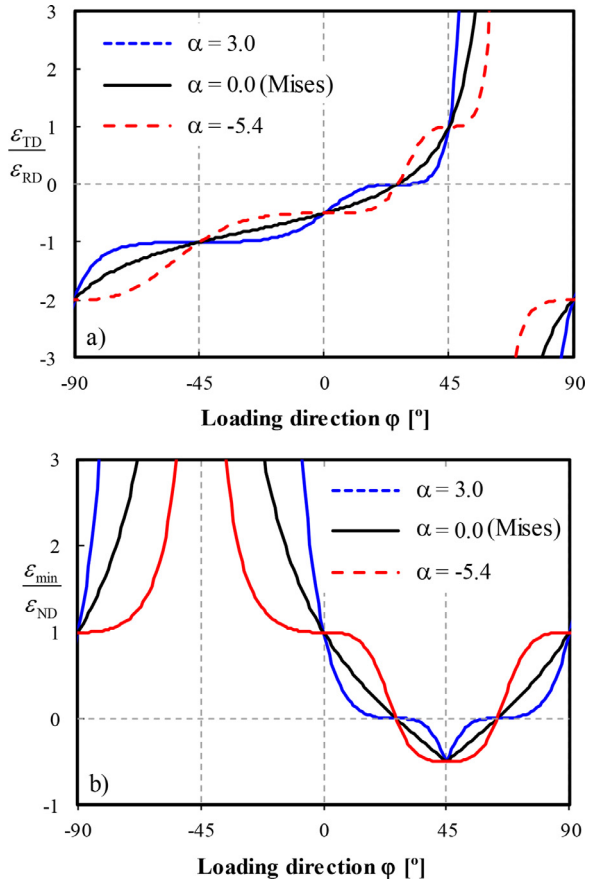

Fig. 12. Strain ratio evolution as a function of the loading direction obtained analytically with the Cazacu [11] yield function (Eq. (1)): (a) $\varepsilon_{TD}/\varepsilon_{RD}$ and (b) $\varepsilon_{min}/\varepsilon_{ND}$.

Fig. 12(b) shows the evolution of the ratio $\varepsilon_{min}/\varepsilon_{ND}$ between the strain with the smallest absolute value (ε_{min}), which can be either ε_{TD} or ε_{RD}, and the thickness strain, $\varepsilon_{zz} \equiv \varepsilon_{ND} = -(\varepsilon_{RD} + \varepsilon_{TD})$. For reference, the ratio $\varepsilon_{min}/\varepsilon_{ND}$ is null for plane strain conditions while for pure shear it has an infinite value. Since the materials points located initially in the flange follow a path close to uniaxial compression (see also Fig. 7) $\varepsilon_{min} = \varepsilon_{rr}$. Note that the $\varepsilon_{min}/\varepsilon_{ND}$ values obtained analytically and plotted in Fig. 12(b) are consistent with the FE results in Fig. 11. It is worth noting that, as previously mentioned, the material points under analysis are mainly subjected to loadings between compression along TD (strain ratio equal to 1.0) and pure shear (corresponding to infinite strain ratio). For the material characterized by $\alpha = 3.0$, the slope of $\varepsilon_{min}/\varepsilon_{ND}$ vs. ϕ is very sharp, meaning that the strain ratio $\varepsilon_{min}/\varepsilon_{ND}$ presents a strong increase even for small values of the radial stress component. On the other hand, for the material characterized by $\alpha = -5.4$, the ratio $\varepsilon_{min}/\varepsilon_{ND}$ presents values closer to 1.0, for a wider range of loading directions (stress ratios).

The results presented in Fig. 12 also provide further understanding of the differences in thickness between the cups, in particular the reason for the differences at the bottom of the cup (i.e. the FE results of Fig. 5). As shown in Fig. 7, the material points located at the bottom of the cup experience stress states between equibiaxial stress ($\phi = 45°$) and plane strain. As shown in Fig. 12(a), the values of the $\varepsilon_{TD}/\varepsilon_{RD}$ ratio for these loading directions are 1.0 and zero, respectively. However, for the material with $\alpha = 3.0$, the $\varepsilon_{TD}/\varepsilon_{RD}$ ratio decreases from 1.0 to zero very rapidly (as seen from the very strong slope), while for the material with $\alpha = -5.4$ this ratio is close to 1.0 for a wide range of loadings (stress ratios). Thus, for the material with $\alpha = -5.4$, same values of the radial strain $\varepsilon_{rr} \equiv \varepsilon_{RD}$ lead to higher values of the circumferential strain $\varepsilon_{\theta\theta} \equiv \varepsilon_{TD}$. This explains the results shown in Fig. 7. On the other hand, Fig. 12(b) shows that for loadings between equibiaxial stress and plane strain, the $\varepsilon_{min}/\varepsilon_{ND}$ ratio evolves from −0.5 to 0. For the material with $\alpha = 3.0$, the $\varepsilon_{min}/\varepsilon_{ND}$ ratio increases from −0.5 to zero with a very strong slope, while for the material with $\alpha = -5.4$ this ratio is closer to −0.5 for a wide range of biaxial loadings. Thus, for the material with $\alpha = -5.4$, the thickness reduction that occurs during forming is much higher than for the other materials.

As shown in Fig. 3, the punch force required to promote the punch movement is higher for the material with $\alpha = -5.4$, which is associated with the fact that the yield surface of this material is external to the yield surface corresponding to the materials with $\alpha = 0$ and $\alpha = 3$, respectively. Therefore, for the same punch displacement the bottom of the cup is subjected to a slightly higher force, which provides an explanation for the increase of the circumferential and radial strains at the centre of the cup bottom (R_0= 0 mm) obtained in the numerical simulations (see Fig. 7). Note that the bottom of the cup does not deform anymore for a punch displacement > 25 mm, which also corresponds to the maximum punch force value.

5. Conclusions

Generally, it is assumed that for isotropic materials the only test needed for characterization of the plastic behaviour is the tensile test, and the data concerning the plastic behaviour in tension is deemed sufficient for prediction of the deformation during forming operations.

Numerical simulations using an isotropic yield criterion that allows to differentiate between isotropic materials that display different ratios, τ_Y/σ_T, between the yield stresses in shear and in uniaxial tension have put into evidence the correlation between this ratio and the deformation during forming. It was shown that the height of a fully drawn cup correlates with this ratio, namely the lower the value of τ_Y/σ_T the greater is the cup height that can be achieved. Moreover, a detailed analysis of the stresses and strains that the material experiences during the forming process was conducted. It was shown that in the flange region the material experiences a variety of loading paths in the compression-tension quadrant (stress states mainly located between uniaxial compression and pure shear).

Accordingly, the plastic strain distribution in the formed part is affected by the shape of the yield locus in this quadrant. The simulations results indicate that for isotropic materials with lower values of the ratio between the yield stresses in shear and in uniaxial tension, compared to von Mises, lead to greater cup heights.

Declaration of Competing Interest

The authors declare that they have no known competing financial interests or personal relationships that could have appeared to influence the work reported in this paper.

Acknowledgments

The authors gratefully acknowledge the financial support of the Portuguese Foundation for Science and Technology (FCT) under the projects with reference PTDC/EME-EME/30592/2017 (POCI-01–0145-FEDER-030592) and PTDC/EME-EME/31243/2017 (POCI-01–0145-FEDER-031243) and by UE/FEDER through the program COMPETE2020 under the project MATIS (CENTRO-01–0145-FEDER-000014) and UIDB/00285/2020. JLA and NC gratefully acknowledge

partial support for this work from the Air Force Research Laboratory (AFRL) under contract FA8651–08-D-0108/52.

Appendix

To study the influence of the choice of the isotropic hardening law on the predictions, simulations were also carried out for the same three materials using a Voce-type law for the variation of the yield stress, Y, with the equivalent plastic strain, i.e.:

$$Y = A - B\exp\left(-C\bar{\varepsilon}^{p}\right) \tag{A.1}$$

where A= 370.9 MPa, B= 247.3 MPa and C = 10.8 (initial yield stress equal to 123.7 MPa). The evolution of the cup height as a function of the angle from the RD is presented in Fig. A.1, while the thickness distribution in the three cups is presented in Fig. A.2. Note that the greatest height is obtained for the material with α = 3.0, while the smallest height corresponds to the material with α = −5.4, i.e. the same trends as in the case when the hardening behaviour is modelled with a power-type law (see Fig. 4).

As previously discussed in Section 3, there is a correlation between the cup's height and the thickness distribution. Note that the material with α = −5.4 presents higher thinning in the bottom region of the cup and the largest increase in the thickness at the wall, while the material with α = 3.0 shows an opposite behaviour, i.e. the same trends observed for the case when hardening is described by the power-law given by Eq. (5) (see Fig. 5). Therefore, irrespective of the isotropic hardening law used the same conclusions can be reached concerning the influence of the ratio between the yield stresses in pure shear and uniaxial tension (i.e. the value of α) on the final cup profile. This indicates that the choice of the isotropic hardening law has a marginal influence; the differences in height and in thickness between the cups being mainly due to the differences in the shape of the yield loci of the respective materials.

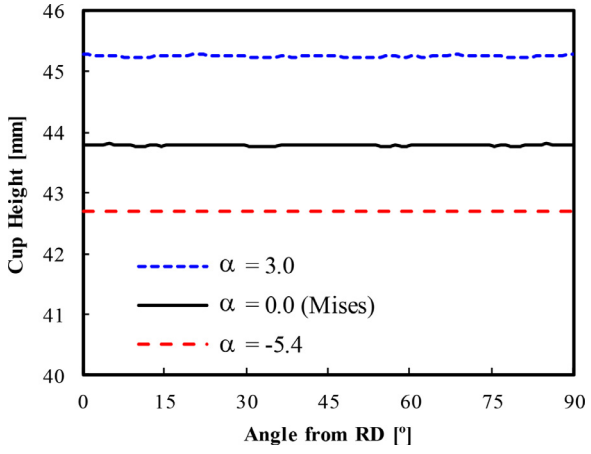

Fig. A.1. Voce-type isotropic hardening law: evolution of the cup height with the angle from the RD for materials characterized by α = −5.4 and α = 3.0 in comparison with a von Mises material (α = 0).

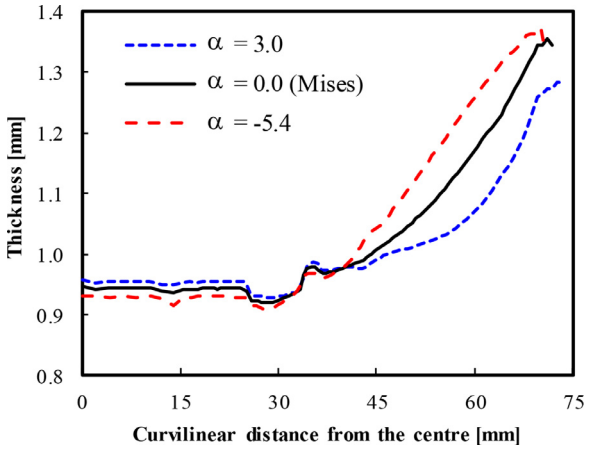

Fig. A.2. Voce-type isotropic hardening law: thickness evolution from the centre to the wall in fully drawn cups of materials characterized by α= −5.4 and α= 3.0 in comparison with a von Mises material (α=0.0).

References

[1] Y. Lou, S. Zhang, J.W. Yoon, A reduced Yld2004 function for modeling of anisotropic plastic deformation of metals under triaxial loading, Int. J. Mech. Sci. 161–162 (2019) 105027, doi:10.1016/j.ijmecsci.2019.105027.
[2] O. Cazacu, New mathematical results and explicit expressions in terms of the stress components of Barlat et al. (1991) orthotropic yield criterion, Int. J. Solids Struct. 176–177 (2019) 86–95, doi:10.1016/j.ijsolstr.2019.05.016.
[3] O. Cazacu, New expressions and calibration strategies for Karafillis and Boyce (1993) yield criterion, Int. J. Solids Struct. 185–186 (2020) 410–422, doi:10.1016/j.ijsolstr.2019.09.004.
[4] F. Barlat, D.J. Lege, J.C. Brem, A six-component yield function for anisotropic materials, Int. J. Plast. 7 (1991) 693–712, doi:10.1016/0749-6419(91)90052-Z.
[5] A.P. Karafillis, M.C. Boyce, A general anisotropic yield criterion using bounds and a transformation weighting tensor, J. Mech. Phys. Solids 41 (1993) 1859–1886, doi:10.1016/0022-5096(93)90073-O.aa.
[6] R. Mises, Mechanics of solid bodies in the plastically-deformable state, Gött. Nachr. Math. Phys. Kl. 1 (1913) 582–592.
[7] H. Tresca, Mémoire sur l'écoulement des corps solides soumis àde fortes pressions, C. R. Acad. Des. Sci. 59 (1864) 754–758.
[8] W. Prager, P.G. Hodge, The Theory of Perfectly Plastic Solids, John Wiley & Sons, 1951.
[9] N.D. Cristescu, Dynamic Plasticity, North Holland, 1967.
[10] D.C. Drucker, Relation of experiments to mathematical theories of plasticity, J. Appl. Mech. 16 (1949).
[11] O. Cazacu, New yield criteria for isotropic and textured metallic materials, Int. J. Solids Struct. 139–140 (2018) 200–210, doi:10.1016/j.ijsolstr.2018.01.036.
[12] O. Cazacu, B. Revil-Baudard, N. Chandola, Plasticity-Damage Couplings: From Single Crystal to Polycrystalline Materials, Springer, 2018, doi:10.1007/978-3-319-92922-4.
[13] T.J.R. Hughes, Generalization of selective integration procedures to anisotropic and nonlinear media, Int. J. Numer. Methods Eng. 15 (1980) 1413–1418, doi:10.1002/nme.1620150914.
[14] L.F. Menezes, C. Teodosiu, Three-dimensional numerical simulation of the deep-drawing process using solid finite elements, J. Mater. Process. Technol. 97 (2000) 100–106, doi:10.1016/S0924-0136(99)00345-3.
[15] D.M. Neto, M.C. Oliveira, L.F. Menezes, Surface smoothing procedures in computational contact mechanics, Arch. Comput. Methods Eng. (2015), doi:10.1007/s11831-015-9159-7.
[16] R. Pearce, Sheet Metal Forming, Springer, 1991.
[17] J.W. Yoon, R.E. Dick, F. Barlat, A new analytical theory for earing generated from anisotropic plasticity, Int. J. Plast. 27 (2011) 1165–1184, doi:10.1016/j.ijplas.2011.01.002.